Interannual variability in the hydrography of the Norwegian Atlantic Current: Frontal versus advective response to atmospheric forcing

K. Richter[1] and S. Maus[2]

[1]   The warm and saline inflow of the North Atlantic Current to the Nordic Seas is highly relevant for the region and the global climate. North of the Greenland-Scotland Ridge, the Norwegian Atlantic Current consists of two 40–60 km wide branches, situated at the slope and 150–200 km offshore, respectively. To interpret changes in these branches in terms of climate variability in the northern North Atlantic, it is important to understand their spatiotemporal response to both atmospheric forcing and advection. We analyzed three decades of synoptic hydrographic observations of the branches' variability, with particular focus on the response to the North Atlantic Oscillation (NAO) and related wind stress curl changes in the Nordic Seas. To do so, we separated the effect of fluctuating position and thickness of the branches from the variability in temperature and salinity in the spatially fluctuating cores. As a rapid response to the NAO we find a deflection of both branches toward the coast which is consistent with an enhanced basin-wide cyclonic circulation. While the immediate correlation between hydrographic properties and the NAO is weak, we find a significant negative correlation when the NAO leads temperature and salinity by 4–6 years. We attribute the overall delayed response to the advection of anomalies generated in the northwestern North Atlantic through NAO induced air-sea interaction and changes in the position of the subpolar front.

1.   Introduction

[2]   The North Atlantic Current (NAC) carries warm and saline water from the Gulf Stream to the northeastern North Atlantic, and is known to be of large importance for the European climate. Once detached from the Gulf Stream near Flemish Cap off North America, it branches again in the central North Atlantic near 30°W, 50°N [*Dietrich et al.*, 1975; *Krauss*, 1986]. It partially recirculates south into the subtropical gyre, and partially continues northeastward. The northerly branch soon splits again, the major part turning north and northwest into the subpolar gyre. A smaller fraction continues north and northeast into the Arctic Mediterranean Seas (ArcMed). There it is transformed into cold dense waters that return to the North Atlantic as deep overflows east and west of Iceland [e.g., *Aagaard et al.*, 1985; *Dickson et al.*, 1996], thus integrating the northern Meridional Overturning Circulation.

[3]   Both the subpolar North Atlantic (SpNA) and the ArcMed respond strongly to the leading mode of North Atlantic atmospheric variability, the North Atlantic Oscillation (NAO) [*Dickson et al.*, 1996, 2000; *Curry and McCartney*, 2001; *Visbeck et al.*, 2003]. Models predict that the response of the SpNA to a high NAO index, an enhanced gyre circulation, takes place within a few years [*Eden and Willebrand*, 2001; *Hátún et al.*, 2005; *Böning et al.*, 2006]. However, its exact timing has been conjectured to depend on the large-scale oceanic state [*Lohmann et al.*, 2009], the model resolution and location of convective areas [*Böning et al.*, 2006; *Frankignoul et al.*, 2009] as well as proper modeling of sea ice and its transport [*Saenko et al.*, 2003; *Herbaut and Houssais*, 2009].

[4]   Within the ArcMed, recent changes related to NAO-high situations were an enhanced oceanic heat transport to the Arctic Ocean [*Adlandsvik and Loeng*, 1991; *Grotefendt et al.*, 1998; *Dickson et al.*, 2000] and a freshening of the Nordic Seas due to increased precipitation and sea ice advection [*Dickson et al.*, 2000; *Blindheim et al.*, 2000; *Vinje*, 2001]. While exchange timescales between the SpNA and ArcMed have been estimated by tracing salinity and temperature anomalies [*Dickson et al.*, 1988; *Belkin et al.*, 1998; *Blindheim et al.*, 2000; *Sundby and Drinkwater*, 2007], model studies indicate that this propagation depends on the amplification of anomalies by atmospheric forcing [*Legutke*, 1991a; *Krahmann et al.*, 2001] and the initial oceanic state [*Häkkinen*, 1999; *Wadley and Bigg*, 2006]. Good spatiotemporal observations are essential to separate the timing of advection and atmospheric forcing.

[1]Bjerknes Centre for Climate Research, University of Bergen, Bergen, Norway.
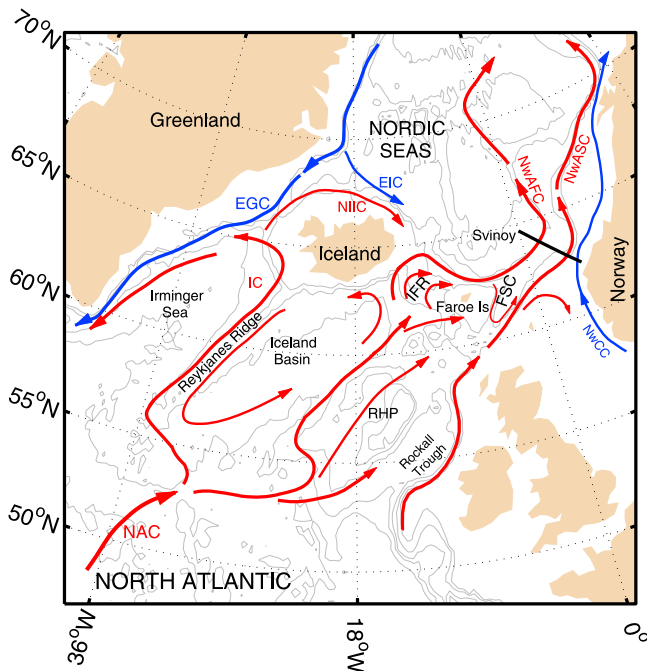[2]Geophysical Institute, University of Bergen, Bergen, Norway.

Figure 1. Bathymetry and surface circulation in the northern North Atlantic. Isobaths are shown for 500, 1000, 2000, 3000, 4000 and 5000 m. Schematic surface currents are based on *Poulain et al.* [1996], *Hansen and Østerhus* [2000] and *Jakobsen et al.* [2003]. The location of the Svinøy section is indicated. NAC, North Atlantic Current; IC, Irminger Current; EGC, East Greenland Current; NIIC, North Icelandic Irminger Current; EIC, East Icelandic Current; RHP, Rockall-Hatton Plateau; IFR, Iceland Faroe Ridge; FSC, Faroe Shetland Channel; NwCC, Norwegian Coastal Current; NwAFC, Norwegian Atlantic Frontal Current; NwASC, Norwegian Atlantic Slope Current.

[5] The NAC inflow branch to the ArcMed has been monitored regularly along the coast of Norway where it is termed the Norwegian Atlantic Current (NwAC). Hydrographic sections have been obtained since the 1950s [*Sælen*, 1959; *Blindheim et al.*, 2000], with particular good spatial and temporal resolution in the Svinøy section that runs from the southern Norwegian shelf northwestward into the central Norwegian Sea (Figure 1). The section has also been the focus of process studies of synoptic ocean inflow variability and mesoscale wave dynamics in the NwAC [*Mysak and Schott*, 1977; *Schott and Bock*, 1980], and is since 1995 monitored by a moored array of current meters [*Orvik et al.*, 2001].

[6] The Svinøy section is of particular interest for studying the inflow from the North Atlantic. At this location, the two branches that derive from NAC inflow west and east of the Faroe Islands are clearly separated as an offshore and inshore branch, respectively [*Blindheim*, 1993; *Orvik et al.*, 2001]. However, the relationship and timing between the branches' hydrographic properties and the NAO proposed so far are not fully consistent. *Blindheim et al.* [2000] analyzed the correlation between the NAO (as well as the related wind stress curl in the Nordic Seas) and the salinity in two close Russian sections (5S and 6S in their Figure 2). They reported a maximum negative relation with the salinity lagging the NAO

by 2–3 years (high NAO and wind stress curl associated with low salinities), and interpreted this in terms of a narrowing of the NwAC. In some contrast, *Mork and Blindheim* [2000] found a maximum negative correlation between the offshore branch salinity and temperature and the NAO without lag (or, as summer data were analyzed, half a year). Also, while *Mork and Blindheim* [2000] had concluded that temperature and salinity in the branches were in opposite phase during summer, *Mork and Skagseth* [2010] rather report an in-phase relationship in the analysis of the extended time series.

[7] In the present work we have extended the mentioned analyses of the Svinøy hydrographic section, based on a longer series with three decades of data. In particular, we performed a spatiotemporal analysis of hydrographic properties to separate the effects of frontal movement and narrowing/deepening from advective anomalies. Our aim is to better understand the relationship between atmospheric forcing and the hydrography in the Svinøy section and to estimate advective timescales between the SpNA and the ArcMed. The observations and methods are presented in Section 2. In Section 3 we describe the main interannual and spatial variability in the section and relate the derived properties to atmospheric forcing in terms of NAO and wind stress curl variability. The results and their implications in terms of climate variability in the ArcMed are discussed in Section 4 and summarized in Section 5.

2. Data and Methods

2.1. Hydrographic Sections

[8] The Svinøy section is approximately 300 km long and runs from 62°N, 5°E on the 200 m shallow southern Norwegian shelf toward 65°N, 0°E in the Norwegian Sea where the water depth is about 2700 m (Figure 1). Hydrographic observations along the section have been taken irregularly since 1955, and at least once a year since 1978 (Figure 2) by the Institute of Marine Research (IMR). The IMR standard section consists of 17 standard stations with the distance between the stations increasing from about 10 km
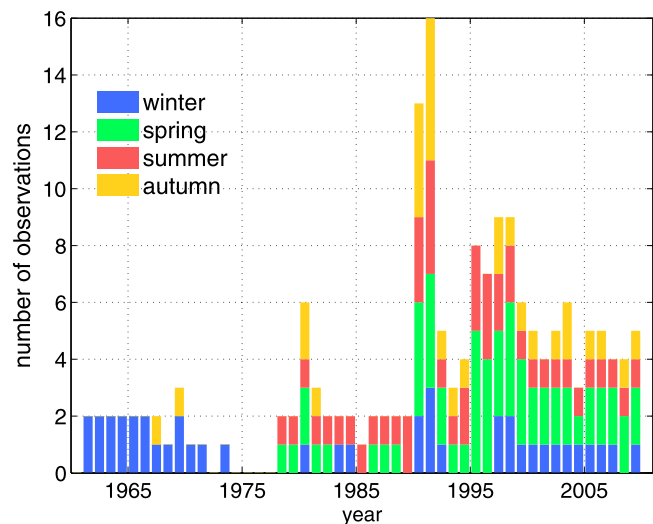

Figure 2. Number of observations in the period 1960–2009. The color coding presents the seasonal coverage (winter, DJF; spring, MAM; summer, JJA; autumn, SON).
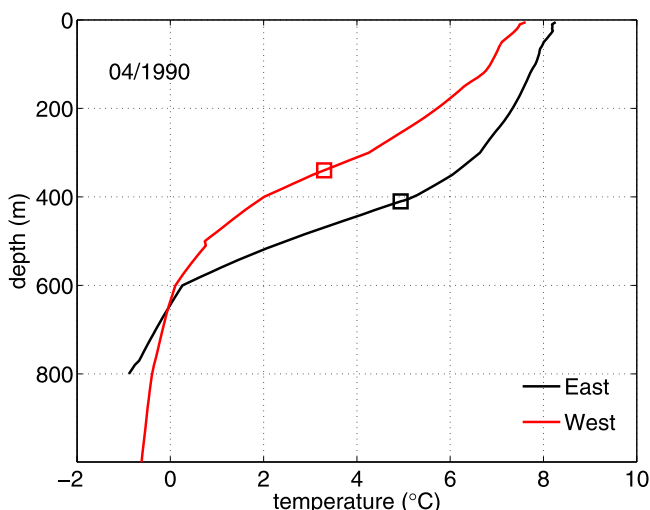
Figure 3. Seasonally mean profile from station 14 (West) and station 10 (East) for spring 1990. The Atlantic layer depth derived from the maximum vertical temperature gradient is shown with open squares. Average core properties are determined from the Atlantic layer depth to a depth of 75 m, to exclude surface effects.

near the shelf break to about 30 km in the open ocean. Since 1978 sampling has been performed at least annually during summer with continuous CTD (conductivity, temperature, depth) profilers with enhanced seasonal coverage since 1990 (Figure 2). In this study, we focus on interannual to sub-decadal variability and use yearly averages.

[9] Due to the irregular sampling, the data set is resampled to seasonal resolution, i.e., a 3-month running mean, centered at January, April, July and October, is applied. In years with no complete seasonal coverage, this will lead to a sea-sonal bias whenever we average the data or properties derived from it. Therefore, the seasonal cycle was removed from the detrended data. The trend was added again once the seasonal variability was removed. We use both the *summer* (JJA) time series (without gaps) and a *yearly* time series with all avail-able data averaged for each year from 1978 to 2009. Yearly averages thus represent observations from December to November.

[10] As mentioned in the introduction, we focus on the eastern (slope, NwASC in Figure 1) and western (open ocean, NwAFC in Figure 1) branches of the section. The properties we study are the position of each branch, salinity S and temperature T as well as the section-wide steric height and its haline and thermal component. The characteristic properties (T, S) are determined within the core of each branch. Rather than using fixed positions, we infer the position of the eastern and western core, X_e and X_w, from their respective maximum in the baroclinic velocity field referenced to 1000 m depth. To do so, the section is divided into a western and an eastern part with stations 12–17 covering the western part and sta-tions 6–10 the eastern part, respectively (see Figure 4 for station numbering). The station east of the maximum bar-oclinic velocity at 50 m depth in each part is taken as the position, X_e and X_w, of the currents. At these positions tem-perature and salinity are averaged between the Atlantic layer depth and 75 m. The maximum baroclinic velocity is by

definition related to strong horizontal gradients in tem-perature and salinity. By choosing the station east of the baroclinic velocity maximum we stay within the branches' cores (40–60 km wide) yet outside the main fronts. To exclude the effect of surface signals on the core properties the upper 75 m are not included. The Atlantic layer depth in the branches, D_e and D_w, is defined as the depth where the ver-tical temperature gradient is at its maximum. Figure 3 illus-trates the procedure according to two temperature profiles in the east (st 10) and west (st 14) in April 1990 as an example.

2.2. Absolute Dynamic Topography From Satellite Altimetry

[11] Maps of absolute dynamic topography from the merged TOPEX/ERS data set are available since 1992 and distributed by the altimeter data processing and distribution center AVISO (http://www.aviso.oceanobs.com/). The pro-vided maps had been corrected for tidal, inverse barometric and dry and wet tropospheric effects [*Le Traon et al.*, 1998]. We extracted the absolute dynamic topography at the location of the Svinøy section, and computed seasonal and yearly data in accordance with the hydrographic data.

2.3. Atmospheric Forcing

[12] We use the NAO index based on the normalized sea level pressure difference between Lisbon, Portugal and Stykkishólmur/Reykjavik, Iceland [*Hurrell*, 1995]. Wind stress curl is computed from the wind stress fields provided by the National Centers for Environmental Prediction — National Center for Atmospheric Research (NCEP-NCAR reanalysis) [*Kalnay et al.*, 1996].

2.4. Steric Height

[13] Steric height has been computed from profiles of potential density using

$$\eta = \int (\rho_0 - \rho)/\rho_0 \; \mathrm{d}z, \qquad (1)$$

where η is steric height and ρ is the in situ density. The integration is from 1000 m depth to the surface. Missing data at depth is replaced with the adjusted long term seasonal mean profile. The reference density ρ_0 is the mean density at 1000 m at each station. According to *Gill and Niiler* [1973], η can be divided into a thermal and a haline component assuming the deviations from a reference temperature and salinity are small. Accordingly,

$$\eta_T = \int \alpha(T, S)(T - T_0) \; \mathrm{d}z$$
$$\eta_S = \int \beta(T, S)(S - S_0) \; \mathrm{d}z, \qquad (2)$$

where α and β are the thermal and haline expansion coeffi-cient of seawater, respectively and are evaluated at the in situ temperature T and salinity S. T_0 and S_0 are the mean tem-perature and salinity, respectively, at 1000 m depth and are computed separately for each station in accordance with the reference density ρ_0. Eastward of station 11 the sea is shal-lower than 1000 m (Figure 4). To allow for comparison of steric height with absolute dynamic topography, temperature and salinity have been extrapolated into the ground at those
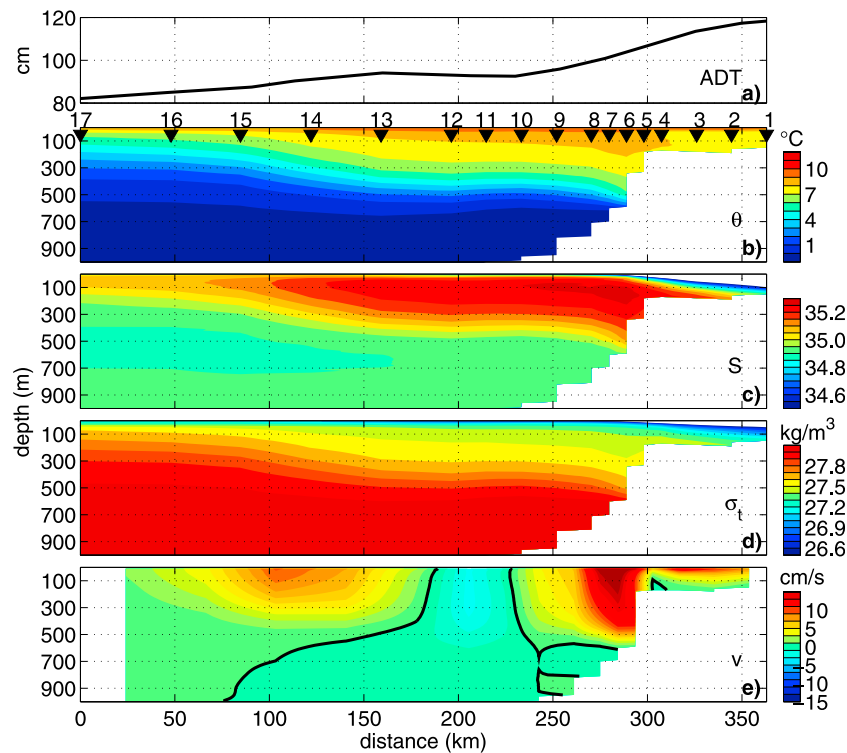
Figure 4. (a) Long term mean of absolute dynamic topography (ADT) along the Svinøy section from altimetry (1993–2009). (b–e) Long term mean of potential temperature θ, salinity S, potential density σ_t and baroclinic velocity v (1978–2009) referenced to 1000 m. The positions of the 17 standard stations are indicated on top of Figure 4b. Yearly data.

stations using the closest 1000 m deep profile. Thus, missing depths at station 10 have been filled with data from station 11, missing data at station 9 with data from the extrapolated station 10 and so forth. This is equivalent to extrapolating the isopycnals horizontally into the slope, thus replacing the solid ground with a fictitious water column with horizontal isopycnals. As for hydrography, the seasonal signal was removed and the 1-yr average was computed.

2.5. Baroclinic Velocity

[14] Baroclinic velocities were computed from sections of potential density and referenced to 1000 m whenever possible using the thermal wind equations. Thus,

$$v(z) = \frac{g}{\rho_0 f} \int_{z_0=1000}^{z} \frac{\partial \rho}{\partial x} \, dz', \qquad (3)$$

where v is the baroclinic velocity, f the Coriolis parameter, ρ_0 a reference density and g the acceleration of gravity. The x-axis is along the section. Over the slope, the horizontal density gradient between two stations was vertically extrapolated into the ground to the depth of the deepest station by using the neighboring offshore station pair. Thus, over the slope the geostrophic velocity is referenced to the depth of the deepest point of two adjacent stations where it vanishes.

3. Results

[15] In this section, we present average hydrographic properties as well as baroclinic velocities of the deseasoned

data set. We then focus on steric height derived from hydrography and compare the results to independent observations from altimetry. This provides an estimate of the quality of the hydrographic observations. Subsequently, properties of the Atlantic water layer are presented and compared to atmospheric forcing.

3.1. Hydrographic Structure

[16] Figure 4 presents the mean hydrographic properties in the Svinøy section for the period 1978–2009, showing vertical sections of potential temperature, salinity, potential density and baroclinic velocity referenced to 1000 m which is well below the Atlantic layer. The corresponding altimeter-derived absolute dynamic topography for a shorter period (1993–2009) is shown in the same figure on top of the hydrography. The Atlantic layer extends as a wedge of warm and saline water from the slope through the whole section on top of a relatively weakly stratified deep layer of colder and fresher water masses. The baroclinic velocity field (Figure 4e) reveals the two-branched current system with the eastern and western branch separated by a weaker recirculation area that is also reflected in the intermediate reversal of the absolute dynamic topography gradient. For a more detailed description of the hydrography and current structure the reader is referred to *Mork and Blindheim* [2000] and *Orvik et al.* [2001] for example.

[17] Figure 5 presents the standard deviations (STD) of hydrographic properties in the Svinøy section over the period 1978–2009. The STD of potential temperature and salinity are not maximal in the cores, but at the base of the Atlantic
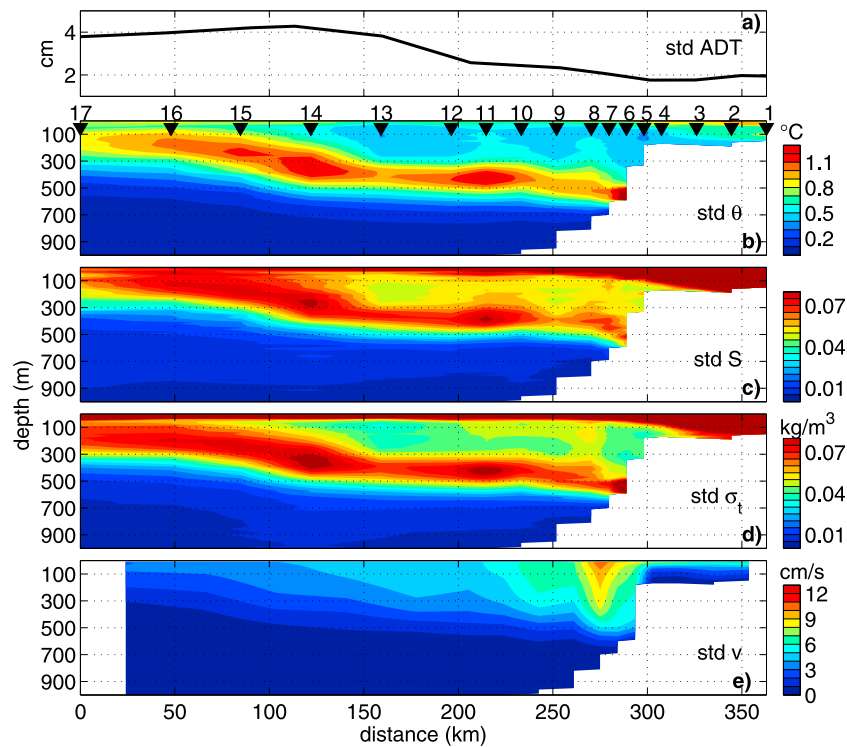
Figure 5. (a) Standard deviation of absolute dynamic topography (ADT) along the Svinøy section from altimetry (1993–2009). (b–e) Standard deviation of potential temperature θ, salinity S, potential density σ_t and baroclinicvelocity v (1978–2009). The positions of the 17 standard stations are indicated on top of Figure 5b. Yearly data.

layer. For potential temperature these maxima are at depths of 300–400 m in the west and 500–550 m in the east (Figure 5b) and correspond to the Atlantic layer depths given in Table 1. For salinity the maximum STD is typically 100 m further up in the water column (Figure 5c). The pattern reflects fluctuations in the thickness of the Atlantic inflow. Note that there is a third STD maximum in T and S located near 210 km at 400 m depth, at the position of the recirculation. The STD is also large near the surface in the west of the section, where the Atlantic layer is very thin. This signal represents the fluctuation in the position of the western core. The fluctuations within the Atlantic water layer and in the deeper layer are significantly lower. The variability in baroclinic velocity is strongest and most distinct in the eastern branch, and decreases gradually offshore (Figure 5e). Recall that all seasonal variations have been removed prior to computing standard deviation.

[18] Sea surface height variability is largest in the western part and decreases gradually toward the shelf. It will be described in more detail below.

3.2. Sea Level Along the Svinøy Section

[19] The hydrographic structure can be further illustrated in terms of STD of the steric field as well as its haline and thermal components. Figure 6a compares the mean steric height and its thermo- and halosteric contributions to the absolute dynamic topography (ADT) derived from altimetry for the period 1993–2009. In the figure the steric height has been set to the same value as the ADT in the west to compare the relative change across the section. The ADT and steric

height changes across the section are similar, indicating that the flow may be described as mainly baroclinic. However, there are noteworthy differences. The stronger ADT gradients in the west and east indicate a stronger northward flow in the western and eastern cores, while the slightly decreasing ADT from 160 to 220 km reflects a stronger southward recirculation than the relative baroclinic velocities yield.

[20] Away from the shelf, the overall increase in steric height toward the east is governed by changes in thermosteric height. The halosteric component decreases gradually toward the east but at the same time the thermosteric component increases at a higher rate. On the shelf, however, it is mainly the halosteric component that contributes to the positive gradient in steric height indicating that the baroclinic part of

Table 1. Mean and Standard Deviation for Atlantic Layer Depth, Position in Terms of Distance From Westernmost Station and Temperature and Salinity in the Western and Eastern Branch[a]

	Mean	SD	Mean JJA	SD JJA
D_w (m)	380	50	370	90
X_w (km)	140	20	130	40
T_w (°C)	6.8	0.4	7.0	0.5
S_w	35.16	0.05	35.15	0.05
D_e (m)	490	70	510	90
X_e (km)	270	10	280	10
T_e (°C)	7.3	0.6	7.2	0.8
S_e	35.20	0.05	35.19	0.06

[a]SD, standard deviation; D, depth; X, position; T, temperature; S, salinity. Yearly averaged data (seasonal variability removed) and summer data (JJA) for comparison.
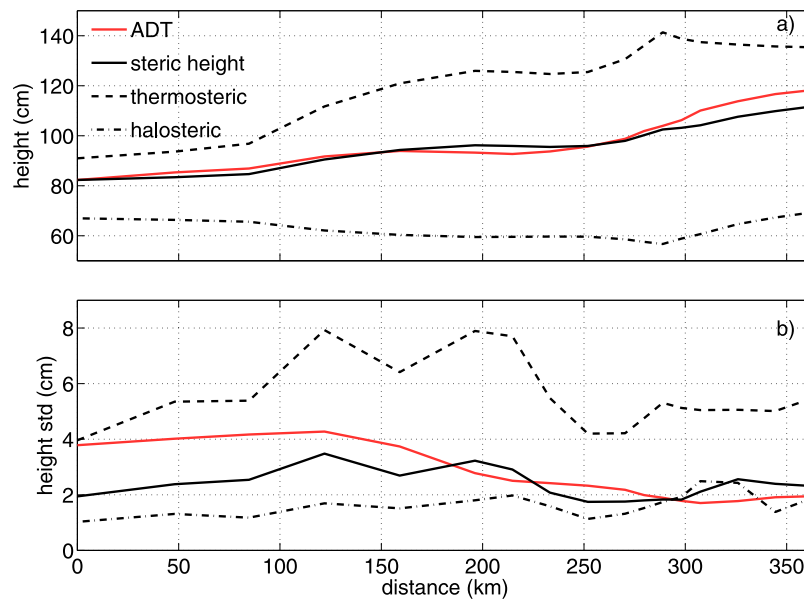
Figure 6. (a) Mean steric height, as well as thermosteric and halosteric contribution over the period 1993–2009. Mean absolute dynamic topography (ADT) from altimetry is shown for comparison. Steric height and its components have been adjusted with the absolute dynamic topography at the westernmost point of the section. Yearly data. (b) As in Figure 6a but for standard deviation and without adjustment.

the Norwegian Coastal Current is driven by its freshwater content.

[21] The variability in steric height is dominated by the thermal component, both in the oceanic and the shelf domain. As the STD in Figure 6b shows, salinity compensates partly and reduces the variability. ADT variability exceeds steric height variability by a factor of 2 in the whole western part of the section. This indicates that currents deeper than 1000 m play a significant role for the transport and sea level variability in the west. The STD in thermosteric height shows two distinct maxima in the west and middle of the section and a less pronounced maximum in the east. They coincide with the two current maxima and the recirculation in baroclinic velocity (Figure 4e). The analysis has been repeated using steric height for the whole period, 1978–2009 (not shown). With the exception of a more pronounced maximum in the east, the general results are unchanged.

[22] Figure 7 further compares the temporal evolution of sea surface height anomalies based on altimetry and steric height along the section. Positive and negative anomalies are alternating on interannual timescales. An oscillation with an approximate period of 4–6 years is most pronounced after 1995 and only weakly visible in the western part during the first half of the record. Halosteric height is dominated by variability on decadal timescales with local maxima in the late 70s and in the early 90s. These maxima coincide with strong minima in the thermosteric height but are not strong enough to balance them completely. The only exception is the beginning of the record when steric height is dominated by a strong maximum in halosteric height. The present analysis suggests that the hydrography of the Svinøy section is of good quality, and may be used to study the variability in the section and its relation to atmospheric forcing in more detail as we will do in the following.

3.3. Properties in the Eastern and Western Parts

[23] In Figure 8 the positions of the eastern and western cores are superposed on the depth of the Atlantic water layer. Temperature and salinity within the eastern and western branch, respectively, are shown in Figure 9. Mean and standard deviations for all properties within the two branches are presented in Table 1 for the yearly and summer data.

[24] Summer values are very close to the annual average for all properties in both branches. The western branch is slightly less saline (0.04) and colder (0.2–0.5°C) than the eastern branch. The layer depths at the core positions, D_e an D_w, agree well with depths inferred from Figure 5 and fluctuate with a similar magnitude, a standard deviation of 90 m in summer, and 50–70 m in the annual mean. Comparison with steric height anomalies (Figure 7) shows that maxima in Atlantic layer depth within the Atlantic water layer coincide with maxima in steric height, e.g., the three maxima after 1995 are clearly visible in both data sets. The shallower western branch (380 m versus 490 m in the east) shows stronger fluctuations in its position X_w compared to the eastern branch. However, as the station spacing increases westward it is more accurate to say that fluctuations in the positions of both cores is in the order of 1–2 station spacing.

[25] To assess the relation between the presented properties, cross-correlation analysis was performed (Table 2). Changes in position of the offshore, western, branch appear to be accompanied by changes in layer depth, deeper Atlantic layer depths being associated with the branch moving eastward. This relationship is most pronounced in the summer data ($r = 0.60$). The corresponding relation between position and depth in the eastern branch is weaker ($r = 0.31$) and statistically not significant. However, the position X_w of the western branch is also negatively correlated with the layer depth D_e in the east ($r = -0.35$). Hence, when the western
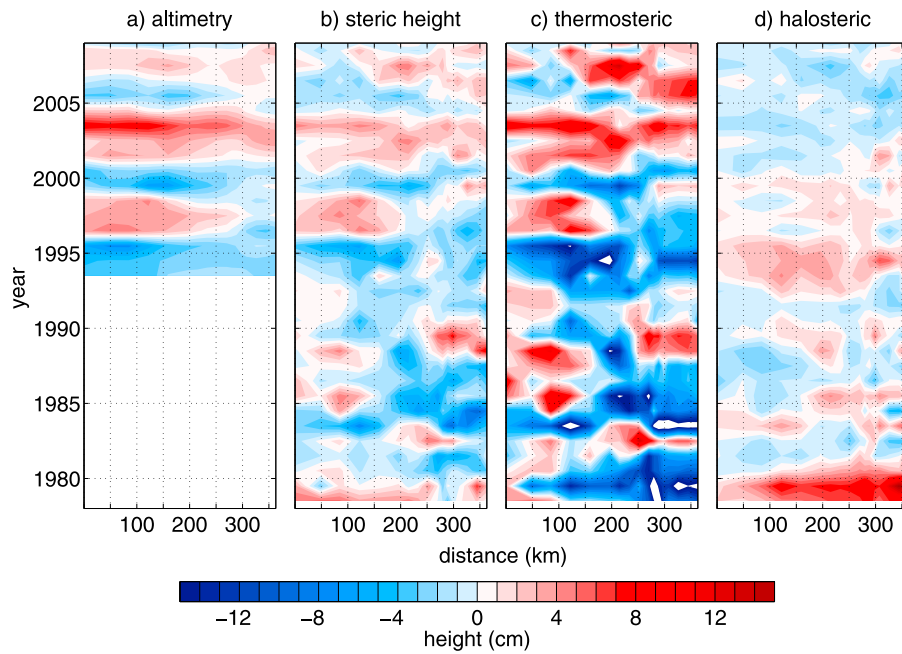
Figure 7. Hovmöller plot of sea surface height anomalies from (a) altimetry, (b) steric height, (c) thermosteric and (d) halosteric height. To be consistent, the anomalies have been computed by removing the mean from 1993 to 2009 from the respective data sets. No altimeter-derived absolute dynamic topography is available prior to late 1992.

branch is closer to the coast, it is deeper, while the eastern branch appears to become shallower.

[26] Temperature and salinity are well correlated within the two branches, with correlation coefficients above 0.70 and highest correlation of 0.85 for eastern temperature and salinity in summer. Cross-branch correlations are weaker. Only salinity is significantly correlated between the cores. Interestingly, the correlation persists when S_e leads S_w by 1 year (r = 0.46, not shown). Figure 9 indicates that the relationship between eastern and western core temperature and salinity appears to be time dependent. After 1995 the

water masses in the east are on average consistently warmer and more saline than in the west, whereas prior to 1995 temperature and salinity in east and west appear to be temporarily in opposite phase. However, the data coverage prior to 1990 is considerably scarcer (Figure 2) and anomalies of different sign are mostly found in years with a single observation. From the overall magnitude of intra-annual variability of anomalies one might suspect that this behavior may be due to noise or synoptic variability. In general, both branches show a similar increase in salinity and temperature over the
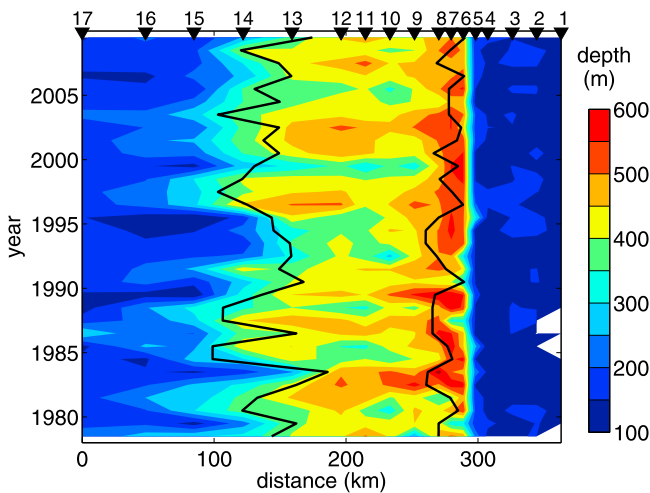

Figure 8. Hovmöller diagram of Atlantic layer depth (color) and positions of the eastern and western branches (lines), respectively. Yearly data. The position of the standard stations is indicated on top.
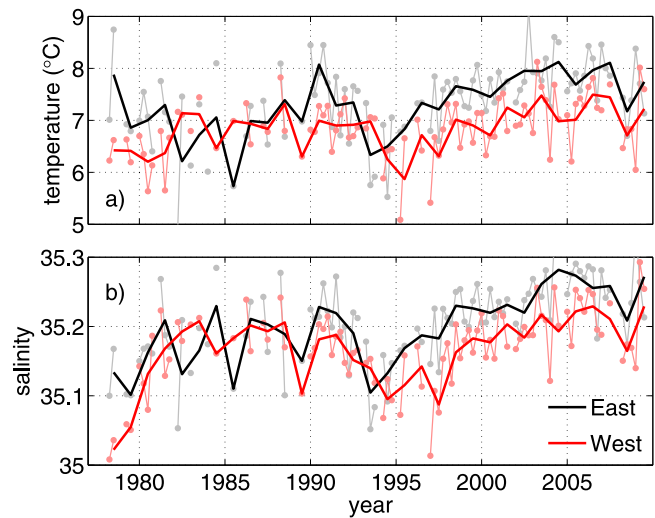

Figure 9. (a) Temperature and (b) salinity in eastern and western branch, respectively. Yearly data (bold lines) and seasonally averaged data with seasonal cycle removed (shaded lines).

Table 2. Correlation Coefficients for Atlantic Layer Depth, Position and Temperature and Salinity in the Western and Eastern Branch[a]

	D_w	X_w	T_w	S_w	D_e	X_e	T_e	S_e
D_w		0.31	0.01	0.06	−0.32	0.22	**0.40**	0.29
X_w	*0.60*		0.18	0.07	**−0.35**	−0.17	0.10	−0.06
T_w	*0.17*	*0.28*		**0.73**	−0.08	−0.06	0.17	0.28
n S_w	*0.20*	*0.17*	*0.71*		0.18	0.06	0	**0.55**
D_e	*−0.26*	**−0.35**	*−0.18*	*0.19*		−0.22	**−0.74**	−0.31
X_e	*−0.02*	*−0.05*	*−0.04*	*0.14*	*0.31*		0.41	0.38
T_e	*0.28*	*0.22*	*0.22*	*0.17*	**−0.66**	*−0.06*		0.68
S_e	*0.25*	*0.15*	*0.20*	**0.46**	*−0.29*	*−0.07*	**0.85**	

[a]D, depth; X, position; T, temperature; S, salinity. A linear trend was removed prior to computing the coefficients. Correlation coefficients with p-value < 0.01 (computed using t-statistics) are given in bold. The part above the diagonal presents correlation coefficients for yearly data while the lower part (italic) is for summer data.

whole period, with pronounced warming and salinification since the mid-1990s.

3.4. Atmosphere-Ocean Covariability

[27] Figure 11 presents the results of a lagged correlation analysis between summer characteristics of the two branches and atmospheric indices, the NAO and the wind stress curl within the Nordic Seas. Since atmospheric forcing in the northern North Atlantic is most pronounced during winter time, we use the winter (DJFM) NAO index as proxy for the *large-scale* atmospheric forcing. As *regional* forcing, we average the wind stress curl over the Nordic Seas for the same season. The wind stress curl is often, but not always, related to the NAO (Figure 10). It is therefore presumably more appropriate when considering the regional forcing.

[28] As data coverage is best, and the noise induced by atmospheric forcing is at its minimum, we use summer (JJA) properties only and correlate them to atmospheric forcing of the previous winters. Thus, a lag of 0 constitutes an actual lag of approximately 6 months.

[29] Overall correlation coefficients are weak, but occasionally significant at the 95% level. The strongest fast response to a positive (negative) NAO is a deflection of the western branch position X_w toward (away from) the coast (Figure 11a). This signal is significant at 0 lag and appears to persist for 1–2 years. While less significant, salinity S_w and geostrophic velocities v_w in the western core increase 0–1 years after an increase in the NAO index. The latter indicates, as the Atlantic layer depth remains unchanged, a sharpening of the front. A similar deflection toward the coast can also be seen in the eastern branch position X_e. In the east, however, the fast (0–1 years) response of salinity S_e and geostrophic velocity v_e are very weak and have the opposite sign compared to the west, with the temperature response (cooling for high NAO) being more pronounced than salinity.

[30] Instantaneous correlation coefficients of western branch properties with the wind stress curl in the Nordic Seas are similar to the NAO correlation (Figure 11b). In the east, the 0–2 year lagged correlation with salinity, temperature and baroclinic velocity is much less stable and coherent than in the west. The only rapid significant correlation in the east is found for the core position, X_e, lagging the NAO by one year. The rapid response in both branches persists for 1–2 years

and appears to be strongest in the position of the branches. Relatively strong correlation coefficients with NAO and Nordic Seas wind stress curl are also found with the position of the eastern branch, the latter lagging the atmospheric forcing by 8 years.

[31] The first significant correlation between salinity and temperature and NAO appears after 4 years. It consists, for high NAO, of a significant freshening and cooling in the eastern branch, and is apparently accompanied by a higher baroclinic velocity V_e. Although not statistically significant, it persists for 2 years and the correlation coefficients for smaller lags indicate, for the NAO, a gradual evolution. In the western branch the lagged correlation of T_w and S_w with the NAO index appears to be delayed, reaching its maximum after 5–6 years. Correlation with the Nordic Seas wind stress curl is slightly less significant and coherent across the properties, yet qualitatively similar, also suggesting the delay between the branches. For lags of 4–6 years, one finds a more offshore position X_w, a shallower depth D_w and a smaller baroclinic velocity V_w in the western branch, while the baroclinic velocity in the eastern branch, V_e, is anomalously large.

4. Discussion

[32] In the present study we analyzed the spatial and temporal variability of the well-monitored hydrographic Svinøy section, through which most of the Atlantic inflow to the Nordic Seas passes in two distinct branches after crossing the Greenland-Scotland Ridge.

[33] There is a high variability in temperature and salinity in the western part of the section related to fluctuations of the western branch's position. There is also high variability at the base of the Atlantic water layer related to fluctuations in the layer depth. The spatial, both vertical and horizontal, variability dominates the standard deviation at fixed stations shown in Figure 5, being 2–3 times larger than in the core properties, thus masking signals purely due to changes in
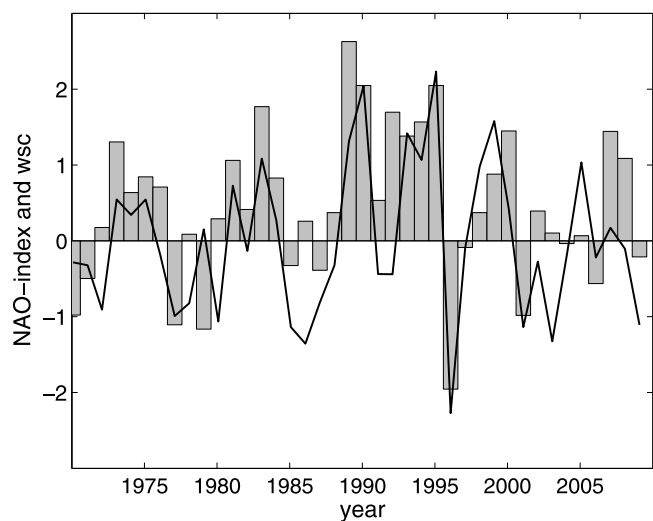

Figure 10. Standardized NAO index (bars) and wind stress curl (line) over the Nordic Seas averaged from December through March. The wind stress curl was computed between 20°W and 20°E, and 60° and 75°N.
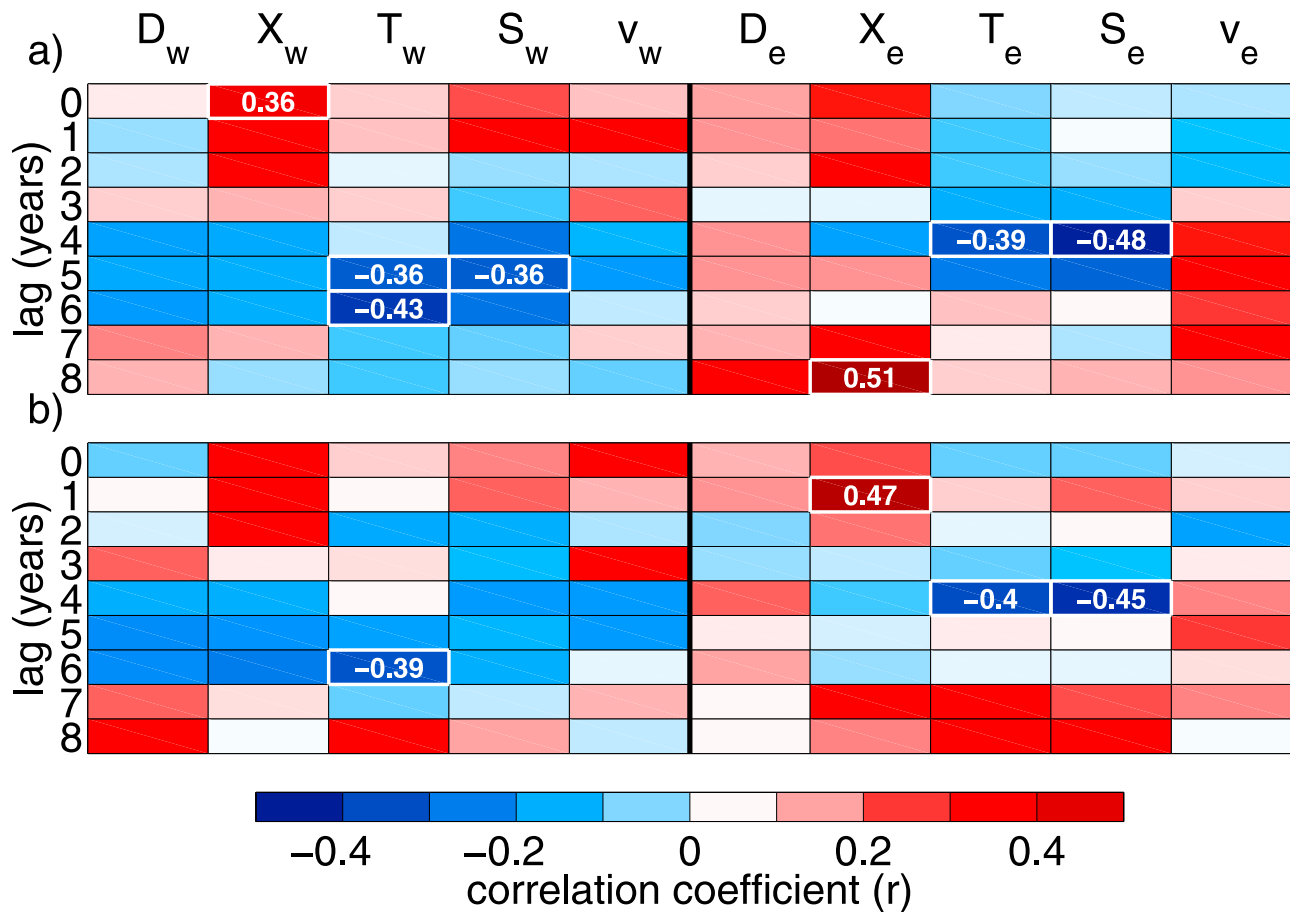
Figure 11. Correlation coefficients of summer Atlantic layer depth D, current position *X*, temperature *T*, salinity *S* and baroclinic velocity *v* at 50 m depth in the two branches for the period 1978–2009 with (a) winter NAO and (b) winter wind stress curl in the Nordic Seas. The analysis was performed for lags of 0–8 years. A linear trend was removed prior to computing the coefficients. Correlation coefficients with p-values < 0.05 are framed with thick white lines and indicated with numbers.

Atlantic water properties. Our approach to trace the baroclinic velocity cores enables us to separate signals due to spatial variability from signals induced by temporal variability. We found that the derived temperature and salinity in the cores are well correlated within each core (Table 2), as has been noted in earlier studies of the data set [*Mork and Blindheim*, 2000; *Mork and Skagseth*, 2010]. However, contrary to the results from *Mork and Blindheim* [2000] who, using fixed-station time series, proposed an opposite-phase relationship between the core properties of the branches, we found no significant correlation coefficients except for a positive correlation between the salinity of the cores. In addition, a warming and salinification is visible in the eastern as well as the western branch. This is consistent with what has been reported from other locations in the Nordic Seas [*Holliday et al.*, 2008; *Hansen et al.*, 2010].

[34] We further analyzed the relation of the branches properties with the NAO and the regionally averaged wind stress curl in the Nordic Seas using lagged correlation analysis (Figures 11a and 11b). The relation between the branches properties and atmospheric forcing is twofold and consists of a fast and a lagged response that will be discussed in the following.

4.1. Rapid Response to Atmospheric Forcing

[35] The most prominent rapid signal is a deflection of both branches toward the coast when winter NAO and Nordic Seas wind stress curl are high. The correlation is at its maximum without lag in the west (NAO), and at 1 year lag in the east (wind stress curl), and persists for 2 years in both branches. This fast response differs from previous studies of different data sources. Using the surface 35 isohaline in the nearby Russian 6S section at 65°N as the position of the westernmost extent of the Norwegian Atlantic Current (NwAC), *Blindheim et al.* [2000] found a maximum correlation when the eastward shift lagged the NAO by 2–3 years. They interpreted this in terms of an intensified circulation of water of polar origin within the Nordic Seas, an intensified East Icelandic Current (EIC, Figure 1) and subsequent freshening of Atlantic Water, driven by the wind field within the Nordic Seas. *Nilsen and Nilsen* [2007] analyzed frontal structures at weather ship Mike, some 100 km north of Svinøy and found a similar response with a maximum lateral shift lagging the NAO by 2 years in apparent agreement with *Blindheim et al.* [2000].

[36] Our results do not support the 2–3 years lagged response proposed earlier. We found a significant lateral shift
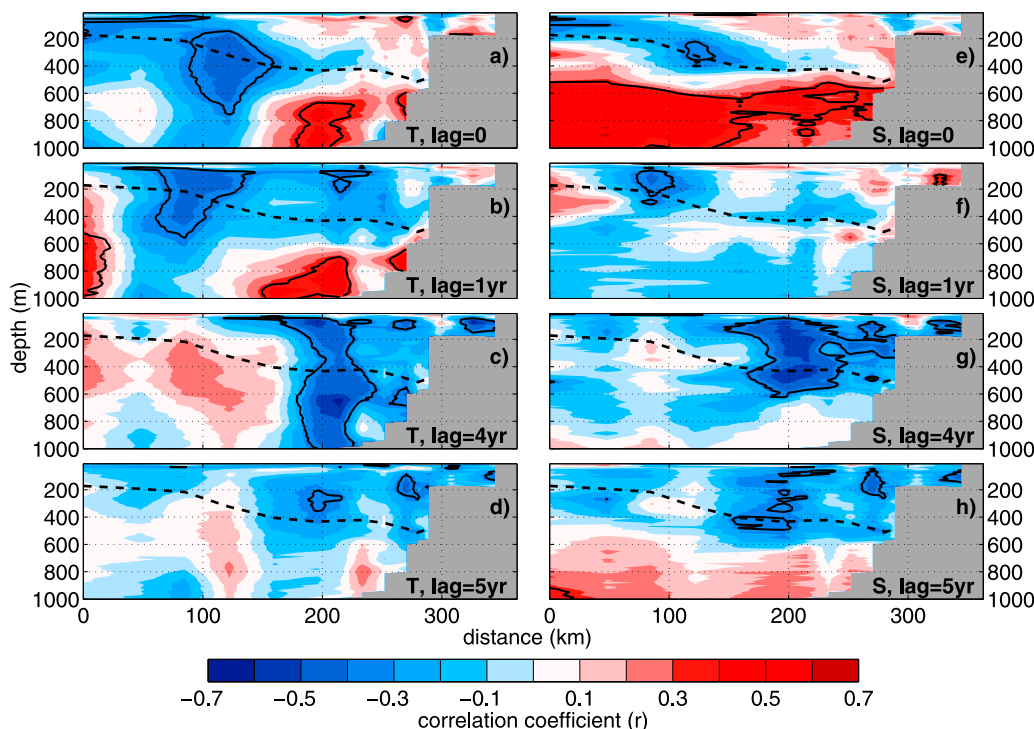
Figure 12. Correlation coefficients of summer (a–d) temperature and (e–h) salinity in the Svinøy section (1978–2009) with winter (DJFM) NAO. The analysis was performed for zero lag (Figures 12a and 12e) and NAO leading hydrography by 1, 4 and 5 years, respectively. A linear trend was removed prior to computing the coefficients. Correlation coefficients statistically significant at the 95% confidence interval are framed with thick black lines. The broken black line represents the mean depth of the Atlantic layer.

in the position of the western branch with 0–1 years lag. Such a rapid response is consistent with an enhanced barotropic gyre circulation within the Nordic Seas driven by the wind stress curl, as proposed on the basis of drifter observations [*Jakobsen et al.*, 2003; *Voet et al.*, 2010], dynamic topography analysis [*Mork and Skagseth*, 2005] and model predictions [*Jónsson*, 1991; *Legutke*, 1991b; *Isachsen et al.*, 2003]. We thus interpret the frontal shift and a narrowing NwAC as a consequence of an enhanced basin-wide cyclonic circulation.

[37] In addition, we expect a rapid local response to the wind-forcing in terms of Ekman fluxes. Owing to increased Ekman transport toward the coast as a response to anomalous wind-forcing, a pressure gradient builds up due to coastal convergence of Ekman transports and strengthens the pressure-driven barotropic circulation. At the same time Ekman transports generate fluxes of heat and freshwater. In Figure 12 we show section-wide correlations between the NAO and temperature and salinity at fixed depths and positions to underline our results. When the hydrography lags the NAO by 0–1 years (Figures 12a, 12b, 12e, and 12f), the frontal shift in the west is the most distinct signal (near 100 km). In the eastern part of the section, the Atlantic layer in the upper 500 m shows a tendency of warmer and more saline water, as a quasi-instantaneous response to a high NAO index (Figures 12a and 12e). This is consistent with correlation maps of freshwater and heat fluxes with the NAO from *Visbeck et al.* [2003] and *Furevik and Nilsen* [2005], showing a near-surface warming and salinification near the coast in the eastern Nordic Seas, mainly as the effect of Ekman-related fluxes.

[38] Finally, we note a significant positive correlation between the NAO and both salinity and temperature below 500 m. Although this signal in the deep water is related to rather weak variability (Figure 5), it is worth mentioning and may be related to changes in deep and intermediate water circulation and exchanges between the basins within the Nordic Seas. It is, however, not discussed any further in this study.

4.2. Delayed Response to Atmospheric Forcing

[39] Figure 11 indicated a significant correlation between temperature/salinity and NAO when the NAO leads the core properties by 4 to 6 years. The correlations peak at 4 years lag in the eastern and 5–6 years in the western branch, respectively, indicating a delay between them. The correlation coefficient between NAO and eastern (western) salinity in Figure 11a is slowly increasing from years 0 (2) to 4 (6) and decreasing afterwards, indicating the advective nature of this signal. Correlation of temperature and salinity with the Nordic Seas wind stress curl are weaker, pointing toward an origin of the signal forced in the northern North Atlantic.

[40] As seen in Figures 12c and 12g, the maximum correlation signal is rather robust and significant between 150 and 300 km and down to 500 m. However, it is noteworthy that it would not have been detected from the very surface fields, which show even a slight positive correlation in terms of T and S. Furthermore, the delayed response in the western branch is not visible in fixed position correlation maps (Figures 12c, 12d, 12g, and 12h), yet was only retrieved by the present front and core tracing approach.

[41] To interpret the delayed response, it is important to know where the anomalies originate. Several studies showed that temperature and salinity anomalies generated in the eastern subpolar gyre persisted along the pathway to the Fram Strait [*Dickson et al.*, 1988; *Belkin et al.*, 1998; *Holliday et al.*, 2008]. The travel time of anomalies from the Faroes to the Svinøy section is, based on observations [e.g., *Furevik*, 2001] and numerical modeling [e.g., *Legutke*, 1991a], typically half a year. Advection time along the NAC to the Faroes has been discussed by several authors. *Sutton and Allen* [1997] demonstrated, by lagged correlation of sea surface temperature fields, a time lag of 3–4 years between a region near 45–55°N and 35–45°W and the Faroe Islands. *Reverdin et al.* [1997] correlated weather ship data for the period 1950–1990. From OWS Charlie (52°45′N and 35°30′W), they found a travel time of 3 years to the Faroe Islands as well as OWS Mike which agrees with 3–4 years obtained from tracing strong salinity anomalies [*Dickson et al.*, 1988; *Belkin et al.*, 1998]. On the modeling side, *Krahmann et al.* [2001] have shown that the propagation of anomalies may depend on the proper forcing fields and model architecture.

[42] Hence, it appears reasonable to consider the region near OWS Charlie as the most likely source area for a signal that reaches Svinøy about 4 years later. Indeed, as shown in detail by *Visbeck et al.* [2003], this region is where the direct NAO-related atmospheric forcing of the ocean is largest in terms of wind stress, net heat and freshwater forcing (including both atmosphere-ocean heat and mass exchange as well as Ekman-induced fluxes). During periods of high NAO the OWS Charlie region in the northwest Atlantic is freshened and cooled.

[43] Another consequence of variable NAO forcing are changes in the position of the subpolar front that affect the relative contributions of cold and fresh subpolar water and warm and saline subtropical water to the Atlantic inflow [*Hátún et al.*, 2005; *Holliday*, 2003], and therefore its properties. Recent observations suggest a northwestward retreat of the subpolar front as a response to low NAO levels [*Bersch*, 2002; *Bersch et al.*, 2007], implying a stronger contribution of water masses of subtropical origin, thus explaining the increasing salinity and temperature of the Atlantic inflow. Observations and model studies [*Eden and Willebrand*, 2001] estimate a response of the subpolar front 1–2 years after changes in atmospheric forcing occur.

[44] Both processes, the generation of anomalies in the western North Atlantic by air-sea interaction and changes in the position of the subpolar front, are part of the North Atlantic's response to NAO variability and create anomalies of the same sign to be advected with the NAC. We cannot distinguish between them in the present study, but the rather long time lag of 4–6 years derived here, suggests that the anomalies originate, and are transferred to the NAC, in the northwestern North Atlantic.

[45] Finally, the correlation analysis indicates that the delayed response in the western branch lags the eastern branch by 1–2 years. This could be related to the different paths of the inflow east and west of the Faroes. The latter is more sluggish, with Atlantic Water first flowing westward south of the Iceland Faroe Ridge (IFR, Figure 1) and, after crossing the ridge, returning eastward [*Poulain et al.*, 1996; *Hansen and Østerhus*, 2000; *Jakobsen et al.*, 2003]. While

of minor magnitude, also the Atlantic inflow west of Iceland may contribute to the delayed arrival of the signal in the western branch. More detailed observations of the circulation around Iceland and the Faroes are needed to clarify it. The delay may also be related to a recirculation within the Nordic Seas, as suggested by *Furevik* [2001] as an interpretation of a 2–3 years time lag between coastal and offshore Atlantic water further north in the Nordic Seas.

5. Conclusion

[46] The variability in temperature and salinity in the two branches of the Norwegian Atlantic Current was explored in terms of its response to regional and large scale atmospheric forcing. By accounting for variable Atlantic layer depth and lateral movement of the current branches, we were able to separate local signals due to frontal movements from advective anomalies.

[47] We found two modes of high correlation between the large scale atmospheric forcing (NAO) and the more local wind stress curl in the Nordic Seas, and the hydrographic properties and their spatial distribution in the Svinøy section: (1) a rapid deflection of the branches position, being at its maximum when lagging the NAO by 0–1 years and (2) a lagged negative correlation of salinity and temperature being maximal after 4 years in the eastern and 5–6 years in the western branch, respectively. While the rapid response is similar for the NAO and Nordic Seas wind stress curl, the delayed response appears to be closer related to variability in the NAO index.

[48] We interpret the rapid response in terms of a spin-up of the basin-wide cyclonic circulation internal to the Nordic Seas while the delayed response is consistent with slow advection of anomalies created in the northwest Atlantic by NAO-related atmosphere-ocean interaction, and/or changes in the position of the subpolar front and thus in water masses contributing to the Atlantic inflow.

[49] The 2–3 years lagged response to atmospheric forcing proposed in earlier work [*Blindheim et al.*, 2000; *Furevik*, 2001; *Nilsen and Nilsen*, 2007] might be related to extensive smoothing of the data in space and time. When this is done, the direct 0–1 years lagged response of the branches position to the NAO-related wind stress curl in the Nordic Seas, is merged and mixed with the 4–6 years lagged response to processes in the North Atlantic, to yield a response time of 2–3 years.

[50] There is indication of the western branch lagging the eastern branch by 1–2 years when considering the delayed response to the NAO. This time-lag might be related to different inflow paths east and west of the Faroes and/or the recirculation of Atlantic Water within the Nordic Seas, the important details of which are still not fully understood. For example, only recently previously unknown current branches east of Greenland [*Pickart et al.*, 2005] and north of Iceland [*Jónsson and Valdimarsson*, 2004] have been reported as important nearby circulation features. Spatial details thus appear to be rather critical to understand the circulation in the vicinity of the Iceland Faroe Ridge, making well resolved long-term sections like the Svinøy section important.

[51] Finally, it is noted that the transport in the Svinøy section is currently monitored with a single current meter

[*Orvik and Skagseth*, 2003]. In view of the discussed deflection of fronts and their persistence during several years, care has to be taken when interpreting these measurements in terms of absolute volume transports.

References

Aagaard, K., J. H. Swift, and E. C. Carmack (1985), Thermohaline circulation in the Arctic Mediterranean Seas, *J. Geophys. Res.*, *90*, 4833–4846.

Adlandsvik, B., and H. Loeng (1991), A study of the climatic system in the Barents Sea, *Polar Res.*, *10*(1), 45–49.

Belkin, I. M., S. Levitus, J. Antonov, and S. A. Malmberg (1998), Great Salinity Anomalies in the North Atlantic, *Prog. Oceanogr.*, *41*(1), 1–68.

Bersch, M. (2002), North Atlantic Oscillation-induced changes of the upper layer circulation in the northern North Atlantic Ocean, *J. Geophys. Res.*, *107*(C10), 3156, doi:10.1029/2001JC000901.

Bersch, M., I. Yashayaev, and K. P. Koltermann (2007), Recent changes of the thermohaline circulation in the subpolar North Atlantic, *Ocean Dyn.*, *57*(3), 223–235.

Blindheim, J. (1993), Seasonal variations in the Atlantic inflow to the Nordic Seas, paper presented at Statutory Meeting, Int. Counc. for the Explor. of the Sea, Dublin.

Blindheim, J., V. Borovkov, B. Hansen, S. A. Malmberg, W. R. Turrell, and S. Østerhus (2000), Upper layer cooling and freshening in the Norwegian Sea in relation to atmospheric forcing, *Deep Sea Res. Part I*, *47*(4), 655–680.

Böning, C. W., M. Scheinert, J. Dengg, A. Biastoch, and A. Funk (2006), Decadal variability of subpolar gyre transport and its reverberation in the North Atlantic overturning, *Geophys. Res. Lett.*, *33*, L21S01, doi:10.1029/2006GL026906.

Curry, R. G., and M. S. McCartney (2001), Ocean gyre circulation changes associated with the North Atlantic Oscillation, *J. Phys. Oceanogr.*, *31*(12), 3374–3400.

Dickson, R. R., J. Meincke, S. A. Malmberg, and A. J. Lee (1988), The Great Salinity Anomaly in the northern North-Atlantic 1968–1982, *Prog. Oceanogr.*, *20*(2), 103–151.

Dickson, R., J. Lazier, J. Meincke, P. Rhines, and J. Swift (1996), Long-term coordinated changes in the convective activity of the North Atlantic, *Prog. Oceanogr.*, *38*(3), 241–295.

Dickson, R. R., T. J. Osborn, J. W. Hurrell, J. Meincke, J. Blindheim, B. Adlandsvik, T. Vinje, G. Alekseev, and W. Maslowski (2000), The Arctic Ocean response to the North Atlantic Oscillation, *J. Clim.*, *13*(15), 2671–2696.

Dietrich, G., K. Kalle, W. Krauss, and G. Siedler (1975), *Allgemeine Meereskunde: Eine Einführung in die Ozeanografie*, 3rd ed., Gebrüder Borntraeger, Berlin.

Eden, C., and J. Willebrand (2001), Mechanism of interannual to decadal variability of the North Atlantic circulation, *J. Clim.*, *14*(10), 2266–2280.

Frankignoul, C., J. Deshayes, and R. Curry (2009), The role of salinity in the decadal variability of the North Atlantic Meridional Overturning Circulation, *Clim. Dyn.*, *33*(6), 777–793.

Furevik, T. (2001), Annual and interannual variability of Atlantic water temperatures in the Norwegian and Barents Seas: 1980–1996, *Deep Sea Res. Part I*, *48*(2), 383–404.

Furevik, T., and J. E. O. Nilsen (2005), Large-scale atmospheric circulation variability and its impacts on the Nordic Seas ocean climate: A review, in *The Nordic Seas: An Integrated Perspective: Oceanography, Climatology, Biogeochemistry, and Modeling, Geophys. Monogr. Ser.*, vol. 158, edited by H. Drange, pp. 105–136, AGU, Washington, D. C.

Gill, A. E., and P. P. Niiler (1973), The theory of the seasonal variability in the ocean, *Deep Sea Res. Oceanogr. Abstr.*, *20*(2), 141–177, doi:10.1016/0011-7471(73)90049-1.

Grotefendt, K., K. Logemann, D. Quadfasel, and S. Ronski (1998), Is the Arctic Ocean warming?, *J. Geophys. Res.*, *103*(C12), 27,679–27,687.

Häkkinen, S. (1999), A simulation of thermohaline effects of a Great Salinity Anomaly, *J. Clim.*, *12*(6), 1781–1795.

Hansen, B., and S. Østerhus (2000), North Atlantic-Nordic Seas exchanges, *Prog. Oceanogr.*, *45*(2), 109–208.

Hansen, B., H. Hátún, R. Kristiansen, S. M. Olsen, and S. Østerhus (2010), Stability and forcing of the Iceland-Faroe inflow of water, heat, and salt to the Arctic, *Ocean Sci.*, *6*(4), 1013–1026.

Hátún, H., A. B. Sandø, H. Drange, B. Hansen, and H. Valdimarsson (2005), Influence of the Atlantic subpolar gyre on the thermohaline circulation, *Science*, *309*(5742), 1841–1844.

Herbaut, C., and M. N. Houssais (2009), Response of the eastern North Atlantic subpolar gyre to the North Atlantic Oscillation, *Geophys. Res. Lett.*, *36*, L17607, doi:10.1029/2009GL039090.

Holliday, N. P. (2003), Air-sea interaction and circulation changes in the northeast Atlantic, *J. Geophys. Res.*, *108*(C8), 3259, doi:10.1029/2002JC001344.

Holliday, N. P., et al. (2008), Reversal of the 1960s to 1990s freshening trend in the northeast North Atlantic and Nordic Seas, *Geophys. Res. Lett.*, *35*, L03614, doi:10.1029/2007GL032675.

Hurrell, J. W. (1995), Decadal trends in the North-Atlantic Oscillation: Regional temperatures and precipitation, *Science*, *269*(5224), 676–679.

Isachsen, P. E., J. H. LaCasce, C. Mauritzen, and S. Häkkinen (2003), Wind-driven variability of the large-scale recirculating flow in the Nordic Seas and Arctic Ocean, *J. Phys. Oceanogr.*, *33*(12), 2534–2550.

Jakobsen, P. K., M. H. Ribergaard, D. Quadfasel, T. Schmith, and C. W. Hughes (2003), Near-surface circulation in the northern North Atlantic as inferred from Lagrangian drifters: Variability from the mesoscale to interannual, *J. Geophys. Res.*, *108*(C8), 3251, doi:10.1029/2002JC001554.

Jónsson, S. (1991), Seasonal and interannual variability of wind stress curl over the Nordic Seas, *J. Geophys. Res.*, *96*(C2), 2649–2659.

Jónsson, S., and H. Valdimarsson (2004), A new path for the Denmark Strait overflow water from the Iceland Sea to Denmark Strait, *Geophys. Res. Lett.*, *31*, L03305, doi:10.1029/2003GL019214.

Kalnay, E., et al. (1996), The NCEP/NCAR 40-year reanalysis project, *Bull. Am. Meteorol. Soc.*, *77*(3), 437–471.

Krahmann, G., M. Visbeck, and G. Reverdin (2001), Formation and propagation of temperature anomalies along the North Atlantic Current, *J. Phys. Oceanogr.*, *31*(5), 1287–1303.

Krauss, W. (1986), The North Atlantic Current, *J. Geophys. Res.*, *91*(C4), 5061–5074.

Legutke, S. (1991a), Numerical experiments relating to the Great Salinity Anomaly of the Seventies in the Greenland and Norwegian Seas, *Prog. Oceanogr.*, *27*(3–4), 341–363.

Legutke, S. (1991b), A numerical investigation of the circulation in the Greenland and Norwegian Seas, *J. Phys. Oceanogr.*, *21*(1), 118–148.

Le Traon, P. Y., F. Nadal, and N. Ducet (1998), An improved mapping method of multisatellite altimeter data, *J. Atmos. Oceanic Technol.*, *15*(2), 522–534.

Lohmann, K., H. Drange, and M. Bentsen (2009), Response of the North Atlantic subpolar gyre to persistent North Atlantic Oscillation like forcing, *Clim. Dyn.*, *32*(2–3), 273–285.

Mork, K. A., and J. Blindheim (2000), Variations in the Atlantic inflow to the Nordic Seas, 1955–1996, *Deep Sea Res. Part I*, *47*(6), 1035–1057.

Mork, K. A., and O. Skagseth (2005), Annual sea surface height variability in the Nordic Seas, in *The Nordic Seas: An Integrated Perspective: Oceanography, Climatology, Biogeochemistry, and Modeling, Geophys. Monogr. Ser.*, vol. 158, edited by H. Drange, pp. 51–64, AGU, Washington, D. C.

Mork, K. A., and O. Skagseth (2010), A quantitative description of the Norwegian Atlantic Current by combining altimetry and hydrography, *Ocean Sci.*, *6*(4), 901–911.

Mysak, L. A., and F. Schott (1977), Evidence for baroclinic instability of the Norwegian current, *J. Geophys. Res.*, *82*(15), 2087–2095.

Nilsen, J. E. O., and F. Nilsen (2007), The Atlantic water flow along the Vøring Plateau: Detecting frontal structures in oceanic station time series, *Deep Sea Res. Part I*, *54*(3), 297–319.

Orvik, K. A., and O. Skagseth (2003), Monitoring the Norwegian Atlantic slope current using a single moored current meter, *Cont. Shelf Res.*, *23*(2), 159–176.

Orvik, K. A., O. Skagseth, and M. Mork (2001), Atlantic inflow to the Nordic Seas: Current structure and volume fluxes from moored current meters, VM-ADCP and SeaSoar-CTD observations, 1995–1999, *Deep Sea Res. Part I*, *48*(4), 937–957.

Pickart, R., D. Torres, and P. Fratantoni (2005), The east Greenland spill jet, *J. Phys. Oceanogr.*, *35*(6), 1037–1053.

Poulain, P. M., A. WarnVarnas, and P. P. Niiler (1996), Near-surface circulation of the Nordic Seas as measured by Lagrangian drifters, *J. Geophys. Res.*, *101*(C8), 18,237–18,258.

Reverdin, G., D. Cayan, and Y. Kushnir (1997), Decadal variability of hydrography in the upper northern North Atlantic in 1948–1990, *J. Geophys. Res.*, *102*(C4), 8505–8531.

Sælen, O. (1959), Studies in the Norwegian Atlantic current. Part 1: The Sognefjord section, *Geophys. Norv.*, *XX*(13), 1–28.

Saenko, O. A., E. C. Wiebe, and A. J. Weaver (2003), North Atlantic response to the above-normal export of sea ice from the Arctic, *J. Geophys. Res.*, *108*(C7), 3224, doi:10.1029/2001JC001166.

Schott, F., and M. Bock (1980), Determination of energy interaction terms and horizontal wavelengths for low-frequency fluctuations in the Norwegian Current, *J. Geophys. Res.*, *85*(C7), 4007–4014.

Sundby, S., and K. Drinkwater (2007), On the mechanisms behind salinity anomaly signals of the northern North Atlantic, *Prog. Oceanogr.*, *73*(2), 190–202.

Sutton, R. T., and M. R. Allen (1997), Decadal predictability of North Atlantic sea surface temperature and climate, *Nature*, *388*(6642), 563–567.

Vinje, T. (2001), Anomalies and trends of sea-ice extent and atmospheric circulation in the Nordic Seas during the period 1864–1998, *J. Clim.*, *14*(3), 255–267.

Visbeck, M., E. Chassignet, R. Curry, T. Delworth, B. Dickson, and G. Krahmann (2003), The ocean's response to North Atlantic Oscillation variability, in *The North Atlantic Oscillation: Climatic Significance and Environmental Impact*, Geophys. Monogr. Ser., vol. 134, edited by J. W. Hurrell et al., pp. 113–146, AGU, Washington, D. C.

Voet, G., D. Quadfasel, K. A. Mork, and H. Søiland (2010), The mid-depth circulation of the Nordic Seas derived from profiling float observations, *Tellus A*, *62*(4), 516–529, doi:10.1111/j.1600-0870.2010.00444.x.

Wadley, M. R., and G. R. Bigg (2006), Are Great Salinity Anomalies advective?, *J. Clim.*, *19*(7), 1080–1088.

S. Maus, Geophysical Institute, University of Bergen, Allegaten 70, N-5007 Bergen, Norway. (sonke.maus@gfi.uib.no)

K. Richter, Bjerknes Centre for Climate Research, University of Bergen, Allegaten 70, N-5007 Bergen, Norway. (kristin.richter@uni.no)